



Efficient photocatalytic degradation of organic water pollutants using V–N-codoped TiO₂ thin films



N. Patel^{a,*}, R. Jaiswal^b, T. Warang^a, G. Scardueli^a, Alpa Dashora^b,
B.L. Ahuja^c, D.C. Kothari^b, A. Miotello^a

^a Dipartimento di Fisica, Università degli Studi di Trento, Via Sommarive 14, Povo, I-38123, Trento, Italy

^b Department of Physics, University of Mumbai, Vidyanagari, Santacruz (E), 400 098, Mumbai, India

^c Department of Physics, M.L. Sukhadia University, 313001, Udaipur, Rajasthan, India

ARTICLE INFO

Article history:

Received 5 October 2013

Received in revised form

18 November 2013

Accepted 20 November 2013

Available online 28 November 2013

Keywords:

Photocatalytic degradation

Visible light

V–N codoped TiO₂

RF-sputtering

ABSTRACT

TiO₂, N-doped TiO₂, V-doped TiO₂, and V–N-codoped TiO₂ thin films have been prepared using RF-magnetron sputtering and their photocatalytic activities have been investigated. The codoping strategy was adopted to decrease both the band gap of TiO₂ and the recombination rate of the photo-generated electron–hole pairs. Low concentration doping with single element (V or N) preserves the anatase dominated phase in TiO₂ film while codoping with V and N produces a mixed phase of nearly equal amount of rutile and anatase as inferred from the XRD and Raman spectroscopy studies. XPS studies reveal that, for N-doped TiO₂ elemental N resides at interstitial lattice positions but codoping with V permits N to reside in both substitutional and interstitial sites in TiO₂ lattice. UV–vis studies indicate that the band gap of TiO₂ (3.2 eV) reduced to 3.0 eV, 2.8 eV and 2.5 eV, by N-doping, V-doping and V–N codoping, respectively. The photocatalytic activity of pure, N-doped, V-doped, and V–N codoped TiO₂ thin films were tested by examining the degradation of methylene blue, chlorophenol and nitrophenol as a function of time. It was observed that the codoped TiO₂ gave the highest photocatalytic activity in comparison to the mono-doped and undoped TiO₂ because of high visible light absorption and possible reduction in the recombination of photo-generated charges. Density of states calculated using density functional theory (DFT) showed that the narrowing of band-gap for the codoped TiO₂ is obtained by the formation of isolated energy levels of V 3d and N 2p states below the conduction band and above the valence band of pure TiO₂, respectively. While for the mono-doped TiO₂ the narrowing of the band gap is only contributed by impurity levels formed near any one of the band edges. It is concluded that for the codoped TiO₂, high visible light absorption is caused by the formation of impurity energy states near both the band edges which also act as the trapping sites for both the photo-generated charges to reduce the recombination process.

© 2013 Elsevier B.V. All rights reserved.

1. Introduction

The toxic organic chemicals, coming from various industrial processes and human activities, contaminate the earth's water which is a serious problem to the living being. The contaminants from industries, mainly dyes, chlorinated benzenes, phenols, etc., are persistent in nature and pollute the aquatic environment.

Photocatalysis is one of the best routes for the degradation of waste water pollutants into harmless by products (H₂O and CO₂) [1]. It is very useful in removing highly toxic and hazardous organic pollutants miscible in water, which are difficult to remove by conventional methods. Even-though most of the organic pollutants

can be degraded by the photocatalysis route, the low efficiency of the reaction demands further research in this field. The development of highly active photo-catalysts with visible light sensitivity is required as it will allow the use of Sun-light for the degradation of waste water pollutants.

TiO₂ semiconductor, with energy band gap of 3.2 eV (anatase phase), shows relatively high reactivity and chemical stability under ultraviolet light [2]. However, for high photocatalytic activity it is necessary to extend the photo-response of TiO₂ to the visible spectrum by modification of its structure and composition. Taking this into consideration, the majority of studies are focused on reducing the band gap of TiO₂ by doping with metals and non-metals to enhance the photocatalytic activity of TiO₂ [3]. Another problem with TiO₂ is the high recombination rate of photo-generated electron–hole pairs which can be limited by introducing charge traps, in the form of dopant element species, for electrons

* Corresponding author. Tel.: +39 461 282012; fax: +39 461 281696.

E-mail addresses: patel@science.unitn.it, nainesh11@gmail.com (N. Patel).

and/or holes, thus prolonging the recombination time [4]. Many attempts have been made to develop TiO_2 photo-catalysts with visible light activity by doping with transition metal ions (Cr, V, Fe, etc.) [5–7]. Another approach to sensitize TiO_2 in visible light is doping with non-metal elements such as nitrogen [8], carbon [9], sulphur [10], iodine [11] etc. which noticeably increase photocatalytic activity of TiO_2 under visible light. Nevertheless, these dopant species when used in large amount can create recombination sites for electrons and holes that limit the photocatalytic activity [12]. On the other hand, low doping content (generally < 2 at%) leads to only small shift in the absorption edge of TiO_2 towards visible region.

Recently it was observed that low concentration co-doping of cations (metals) and anions (non-metals) in TiO_2 are able to both enhance the visible light absorption efficiency and reduce the recombination of the photo-generated charges. Cong et al. [5] found that TiO_2 nano-particles codoped with N and Fe(III) show greatly-enhanced visible light irradiated photocatalytic activities. Li et al. [13] reported that N and F codoped TiO_2 had higher visible light activity than N-doped or F-doped TiO_2 . Liu et al. [14] and Gu et al. [15] have synthesized codoped TiO_2 with V and N and observed an enhancement in the degradation of methylene blue dye and of pentachlorophenol, respectively, as compared to the single-element doped TiO_2 . Wen et al. [16] reported the synthesis of I and F codoped TiO_2 and studied photocatalytic degradation of methylene blue solution. The synergetic effects on the optical absorption, crystallinity, and activity of TiO_2 due to co-doping of two non-metals like N, S atoms [17] and C, N atoms [18] have also been reported. In our recent work [19], V–N codoped TiO_2 nano-powders, synthesized by sol–gel method, were able to efficiently degrade Rhodamine dye under visible light due to the synergic effect created by V and N species. However, the powders have problems related to separation and aggregation. Also, powders cannot be used in industrial waste water treatment plant based on continuous flow system. Thin film photo-catalyst deposited on appropriate support can be easily recovered and reused, thus solving problems related to powder catalysts.

Thus, in the present study V and N codoped TiO_2 photocatalyst is synthesized in the form of thin film catalyst to study the photocatalytic performance, under visible light irradiation, in degradation of three organic pollutants, namely 4-Nitrophenol (4-NP), 4-Chlorophenol (4-CP), and Methylene Blue (MB) dye, different from that investigated in our past work [19]. In addition, DFT calculation was also performed to understand the origin of the band gap narrowing. The detailed analytical characterization and the photocatalytic results showed that V and N codoped TiO_2 thin films are superior to mono-doped and undoped TiO_2 for the enhanced photocatalytic activity. By testing the recyclability of the thin film catalyst we realized that the present form is suitable for the industrial waste water treatment application which is not viable with powder catalyst.

2. Experimental and computational methods

2.1. Catalyst preparation

RF-magnetron sputtering was used to synthesize pure TiO_2 , N-doped TiO_2 , V-doped TiO_2 , and V–N codoped TiO_2 thin films. For undoped TiO_2 films, pure TiO_2 disc (99.99%) and pure Ar (99.99%) were used as sputtering target and working gas, respectively. Base pressure of less than 3×10^{-5} Pa and working Ar pressure of 0.8 Pa were used for the deposition. Before the deposition, the TiO_2 target was pre-sputtered for 20 min in order to remove any surface contamination. TiO_2 target was sputtered on both glass and Si (100) substrates at room temperature using RF power of 150 W. The sample and target distance was maintained at 5 cm for all the samples.

Nitrogen gas was introduced during the deposition of N-doped TiO_2 films by maintaining the Ar/N_2 flow rate equal to 3. V-doped TiO_2 films were synthesized by partially covering the TiO_2 target surface with small V-metal pieces. The combination of the above two strategies was utilized to deposit V–N codoped TiO_2 thin film. After deposition, all TiO_2 samples were annealed in air at 500 °C for 2 h. Our past investigation with V–N-codoped TiO_2 powder showed that dopants concentration must be kept low and concentration of N atoms should be about 2 times than that of V atoms to obtain enhanced photocatalytic activity [19]. Thus by varying the number of V-metal pieces on TiO_2 target and Ar/N_2 flow ratio in the chamber the concentration of dopants was optimized to 1 at% for V and 2 at% for N dopant.

2.2. Catalyst characterization

The structural characterization of the deposited samples was carried out by conventional X-ray diffraction (XRD), $\text{Cu } K_\alpha$ radiation ($\lambda = 1.5414 \text{ \AA}$), in Bragg–Brentano (θ – 2θ) configuration. Raman spectra were recorded using HORIBA Jobin Yvon Lab RAMA ramis Raman spectrometer with diode pumped solid state laser at 532 nm. X-ray photoelectron spectra (XPS) were acquired using a Kratos AXIS Ultra^{DL} instrument equipped with a monochromatic Al K_α (1486.6 eV) X-Ray source and a hemispherical analyzer. No electrical charge compensation was required to perform XPS analysis. Survey spectra were measured over a binding energy (BE) range from 0 to 1200 eV using a constant pass energy of 160 eV and a step size of 0.5 eV, while Ti 2p, V 2p, O 1s, N 1s and C 1s core levels were acquired using a constant pass energy of 20 eV and a step size of 0.1 eV. All the binding energies were referred to the C 1s main peak at the lower-BE-side of the C 1s envelope in order to take the O 1s main peak at the lower-BE-side of the O 1s envelope at 529.9 eV. Data analysis was performed by using Kratos Visual Processing software. Different background-types (linear, Shirley and Tougaard) and different Gauss-Lorentzian line shape functions were tested in order to evaluate any differences in peak areas and to minimize the residual curve. Optical measurements of all TiO_2 films were performed using VARIAN Cary 5000 UV–Vis-NIR spectrophotometer with incoming beam incident normally. To obtain the absorbance spectra of samples deposited on glass slides, the measurements were performed in the photon energy range between 1.0 to 4.5 eV.

2.3. Photocatalytic activity measurement

The photocatalytic activity of all TiO_2 thin films was tested by degradation of water pollutants. 4-Nitrophenol (4-NP), 4-Chlorophenol (4-CP), and Methylene Blue dye (MB, Alfa Aesar), dissolved in water solution were used as organic pollutants. Undoped and doped TiO_2 films were dipped in pollutants solution and stirred in dark for 30 min to establish adsorption equilibrium between the solution and the catalysts. Later, for the photocatalytic reaction, each pollutant solutions were irradiated by 150 W tungsten halogen lamp (which consists of mostly visible light spectrum in the range of 350–900 nm) in the presence of photo-catalyst. No oxidants or no aerated conditions were used for the photocatalytic measurements. After established time intervals, 1 ml aqueous solution was filtered out from the reactor vessel. The UV–visible absorption measurements of the filtered solution were carried out using a spectrophotometer (Cary 5000). The concentration of each pollutant was estimated by measuring the normalized intensity of the absorption peak in UV–visible range and plotting it as a function of time of irradiation. All the photo-catalysis experiments were performed at room temperature, maintained constant by using a cooling system operated with a continuous water flow. The pH of the solution was maintained neutral during all the

photocatalytic measurements. The reusability property of the codoped TiO_2 thin film photo-catalyst was further established by collecting the photo-catalyst after the degradation reaction and washing with distilled water before reintroducing into the MB dye solution to acquire another run. The sample was recycled 4 times in a similar manner.

2.4. Computational model and method

Total and partial density of states of pure, mono- and codoped- TiO_2 were computed using full potential linearized augmented plane wave (FP-LAPW) method within the density functional theory (DFT) as embodied in WIEN2k code [20]. The FP-LAPW combines the choice of the LAPW basis set with the treatment of full-potential. In this code, the wave function, charge density and potential are expanded by spherical harmonic functions inside non-overlapping spheres surrounding the atomic sites (muffin-tin, MT, spheres) and by a plane wave basis set in the remaining space of the unit cell (interstitial region). The exchange and correlation potentials given by Perdew et al. [21] within the Generalized Gradient Approximation (GGA) were used. To overcome the problem of band gap underestimation by standard GGA method, modified Becke–Johnson (mBJ) [22] potential was also included in the present computations. For pure anatase TiO_2 , lattice parameters were considered as $a = 3.838$ and $c = 9.642$ Å as optimized by Rubio-Ponce et al. [23] using FP-LAPW scheme. For the computation of V–N codoped TiO_2 , the $3 \times 3 \times 3$ super cell of TiO_2 were considered to generate 54 atoms of Ti and 108 atoms of O. One Ti atom was replaced by one V atom and four O atoms were replaced by four N atoms. Three separate calculations were performed with different doping at Ti and O site as $\text{Ti}_{0.98}(\text{V})_{0.02}\text{O}_2$, $\text{Ti}_{0.96}\text{N}_{0.04}$, and $\text{Ti}_{0.98}\text{V}_{0.02}\text{O}_{1.96}\text{N}_{0.04}$. All the systems were relaxed by minimizing the forces acting on each atom until the forces on each atom reach values less than 5 mRy/a.u. The self-consistent field tolerance was set to 10^{-4} Ry.

For the present computations, radii for MT spheres for both Ti and V atoms were selected as 1.73 a.u. while for O and N atoms it was set to 1.53 a.u. The \mathbf{k} -point sampling of the Brillouin zone (BZ) was set as $14 \times 14 \times 14$ and $5 \times 5 \times 5$ for pure TiO_2 and other doped and codoped compounds, respectively. The basis-set was controlled by a cut-off parameter, $R_{\text{mt}}K_{\text{max}} = 7$ (where, R_{mt} is the smallest atomic sphere radius in the unit cell and K_{max} is the magnitude of the largest K vector). The maximum radial expansion, l_{max} , inside the MT sphere was set to 10 while the cutoff for charge density, G_{max} , was set to 12 in all the systems.

3. Results and discussion

Fig. 1 represents the XRD pattern of pure, N-doped, V-doped, and V–N codoped TiO_2 thin films. The peaks observed at 25.3° , 37.7° , 48.1° , 53.8° , and 55.1° in all TiO_2 films corresponds to (1 0 1), (0 0 4), (2 0 0), (1 0 5), and (2 1 1) planes of anatase phase of TiO_2 . In addition, broad peaks due to rutile TiO_2 are also observed at 27.4° and 36.1° . This shows that mixed phase of anatase-rutile is

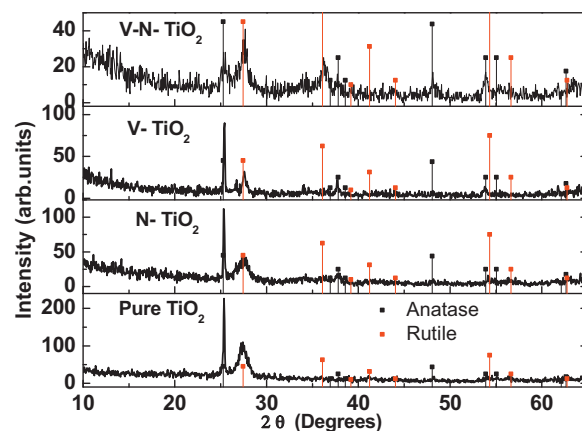


Fig. 1. XRD pattern of pure, N-doped, V-doped, and V–N codoped TiO_2 thin films.

present in all the TiO_2 films. The crystallite grain-sizes of anatase and rutile phases for all the samples were calculated using the Debye–Scherrer equation from the peaks (1 0 1)-anatase at 25.3° and (1 1 0)-rutile at 27.4° , respectively, and summarized in Table 1. The weight fraction of the anatase phase calculated from the intensity ratio of the anatase (1 0 1) to rutile (1 1 0) peak is also reported in Table 1. For undoped and mono-doped TiO_2 , the anatase phase with nanocrystalline structure is more prominent than the rutile phase. TiO_2 codoped with V and N exhibits peak of the rutile phase prevailing over the anatase phase. The crystalline degree of TiO_2 is also decreased by codoping as indicated by the broader appearance of the main anatase peak at 25.3° . For codoped TiO_2 , the presence of V^{4+} or V^{5+} ions and of N^{3-} ions permits the rearrangement of Ti^{4+} and O^{2-} ions in the lattice which favors the anatase to rutile phase transformation [24]. In the case of single V- or N-doped TiO_2 , the low doping concentration is not sufficient for rutile phase development.

In order to investigate the structural properties of the photocatalyst surface, Raman spectra were acquired and presented in Fig. 2 for pure, N-doped, V-doped and V–N-codoped TiO_2 thin films. All the films clearly display five bands located at approximately 144, 197, 396, 517 and 639 cm^{-1} corresponding to the E_g , E_g , B_{1g} , A_{1g} , and B_{2g} , vibrational modes of the anatase phase, respectively [25]. In addition to these five bands of the anatase phase, broad peak centered at 445 cm^{-1} due to the rutile phase is also evident in all the films of TiO_2 [25] indicating the presence of a mixed anatase-rutile phase on the surface. The main anatase peak at 144 cm^{-1} shows broadening as well as the decrease in intensity for the V–N codoped TiO_2 film. This broadening signifies that after V and N codoping the crystalline degree of the TiO_2 film is decreased noticeably in agreement with the XRD results.

XPS was used to investigate the chemical state of the dopant species incorporated into the TiO_2 lattice. The core level energies of Ti 2p, V 2p, O 1s and N 1s of all the photo-catalyst films are reported in Fig. 3. For each sample, Ti 2p core level shows a typical doublet of TiO_2 compound with binding energy (BE) value in the range of 458.7–458.6 and 464.5–464.4 eV, assigned to $\text{Ti } 2p_{3/2}$ and

Table 1
Crystallite sizes, weight fraction of the anatase phase, band gap and apparent reaction rate constants of 4-CP, 4-NP and MB degradation for the undoped and doped TiO_2 films deposited using RF-sputtering.

TiO_2 thin films	Crystallite size from XRD		Weight fraction of anatase (x_A) (%)	Band gap (eV)	Apparent reaction rate constant ($\times 10^{-2}$) (min^{-1})		
	Anatase (1 0 1) (nm)	Rutile (1 1 0) (nm)			4-CP	4-NP	MB
Pure TiO_2	~57	~9	~75	~3.12	0.6	0.33	1.0
N- TiO_2	~53	~6	~72	~3.01	0.7	0.48	1.3
V- TiO_2	~55	~11	~71	~2.86	0.95	0.72	2.0
V–N- TiO_2	~9	~8	~41	~2.52	1.12	0.94	2.6

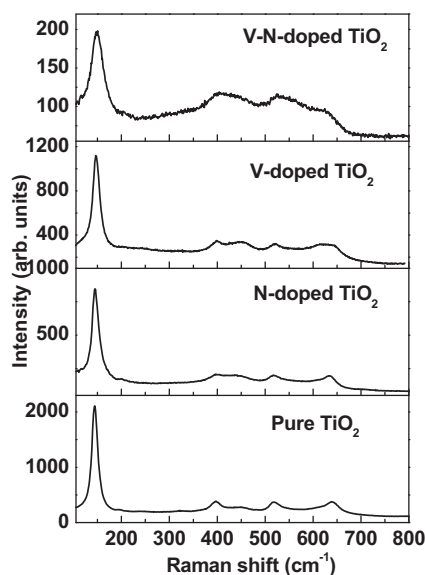


Fig. 2. Raman spectra of pure, N-doped, V-doped, and V–N codoped TiO_2 thin films.

$\text{Ti}2p_{1/2}$, respectively. The comparison between the $\text{Ti} 2p$ doublet positions, widths and shapes in the spectra acquired, indicate that the $\text{Ti} 2p$ core levels are due to the Ti^{4+} oxidation state of the Ti. For all the deposited films, the $\text{O} 1s$ spectra acquired (Fig. 3) suggest the co-presence of different oxidation states, which include M–O (M = Metal, i.e. V and/or Ti) species (as indicated by the main peak position of the $\text{O} 1s$ envelope at 529.9 eV), and hydroxyl ($-\text{OH}$) groups (as indicated by the presence of the shoulder between 533.2 and 531.5 eV).

Fig. 3 shows the $\text{N} 1s$ core level XPS spectra of the N-doped film, with and without V-codoping. For the N-doped film without V-codoping, the $\text{N} 1s$ spectrum shows two main broad peaks

centered at 402.5 and 396.2 eV. Former peak is attributed to interstitial occupation of N in TiO_2 lattice and NO-like species, while later peak is assigned to the formation of Ti–N bond without attached oxygen [26,27]. However, for V–N codoped TiO_2 the peak at 396.2 eV is absent, instead peak at higher binding energies at 399.7 eV is observed which is attributed to O–Ti–N linkage formed by substitutionally replacement of O by N atom in the TiO_2 lattice. Since the presence of O atom reduces the electron density around N atom, the $\text{N} 1s$ peak is shifted towards the higher binding energy [28]. Peak at higher BE centered at 403.5 eV is due to interstitial occupation of N in TiO_2 lattice and oxidized N species (NO) to form Ti–O–N and Ti–O–N–O linkage, respectively. These results indicate that for N-doped TiO_2 , N occupies only interstitial sites in the lattice, while co-doping with V permits N to reside in both substitutional and interstitial sites in TiO_2 lattice which induces higher visible light sensitivity as proposed by Ma et al. [29].

In V-doped and V–N codoped TiO_2 films, the $\text{V} 2p$ core level shows two broad peaks centered at 516.8 and 523.6 eV corresponding to $\text{V}2p_{3/2}$ and $\text{V}2p_{1/2}$ configuration, respectively. Despite the peak symmetry, the co-presence of the V^{5+} oxidation state ($\text{V}2p_{3/2}$ at 517.6 eV), and/or the V^{3+} oxidation state ($\text{V} 2p_{3/2}$ at 515.7 eV) cannot be completely excluded, because of the difficulty of the background evaluation due to a very noisy spectrum and the proximity of the very intense $\text{O}1s$ signal. Thus the broad peak in $\text{V}2p_{3/2}$ level was deconvoluted into two peaks having binding energy values of 517.9 and 516.6 eV attributed to V^{5+} and V^{4+} states, respectively [30,31]. This indicates that V exists in TiO_2 in the form of V^{5+} and V^{4+} , with higher quantity of V^{4+} ions as inferred from the area under the peak in XPS spectrum. Indeed, the effective diameter of V^{4+} ions is comparable to that of Ti^{4+} ions; thus it is certainly possible that during sputter deposition the metal ions emitted from the target with kinetic energy of some 10 eV might be able to replace Ti^{4+} ions in the lattice of TiO_2 . On the contrary, V^{5+} may be present on the TiO_2 surface in the form of V_2O_5 phase. Through XPS analysis the concentration of V and N is estimated to be around 1 and 2 at%, respectively for mono-doped and codoped TiO_2 .

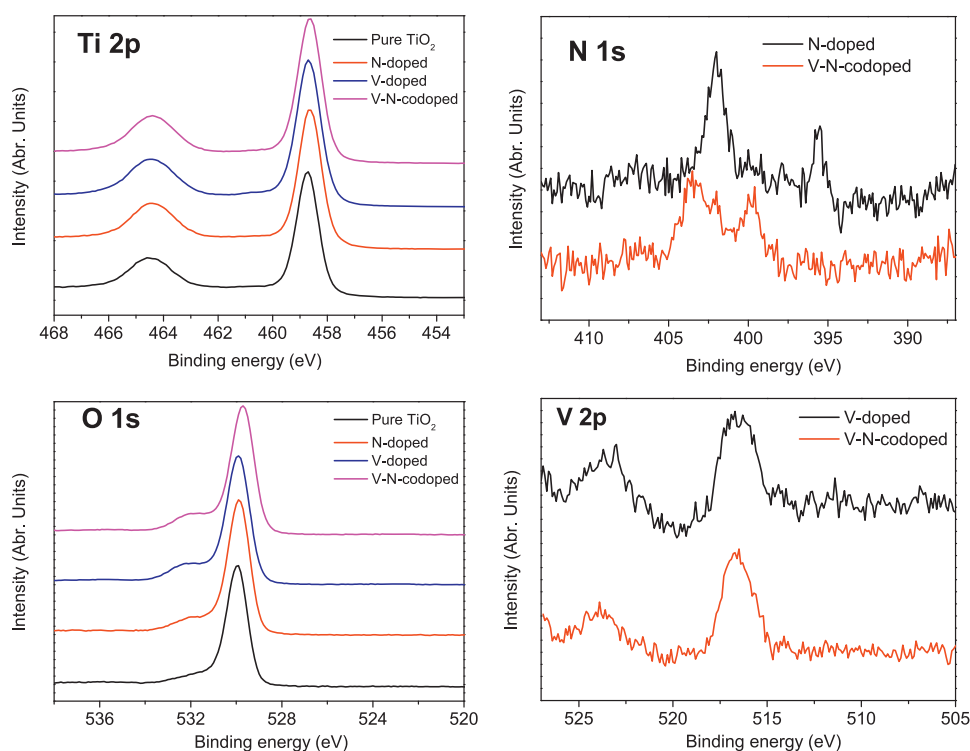


Fig. 3. XPS spectra of $\text{Ti} 2p$, $\text{O} 1s$, $\text{V} 2p$ and $\text{N} 1s$ levels of pure, N-doped, V-doped, and V–N codoped TiO_2 thin films.

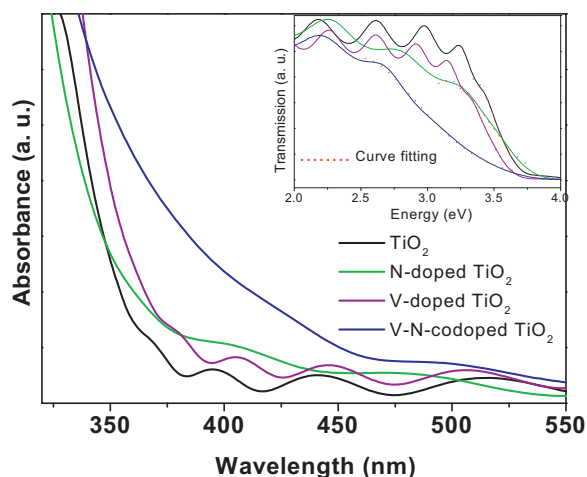


Fig. 4. UV–visible absorption spectra of pure, N-doped, V-doped, and V–N codoped TiO₂ thin films. Inset shows the same spectra in Transmission mode with the fitting of absorption edge with Eq. (1) to obtain band gap values.

Fig. 4 shows the optical absorption spectra of undoped and doped TiO₂ films. It is clearly visible from the spectra that the tail of absorption edge gets significantly shifted to the visible region after co-doping with V and N in TiO₂ as compared to single-element doped and undoped TiO₂. The band gap values were obtained by fitting the absorption edge using the following equation [32]:

$$\ln T = \ln T_0 - C \frac{(\hbar\omega - E_g)^\nu}{\hbar\omega} \quad (1)$$

where E_g is the band gap, C is a constant, and T_0 is the optical transmission of the substrate. Depending on the type of transition, ν assumes different values: for direct, allowed (forbidden) transitions $\nu = 1/2$ ($\nu = 3/2$) and for indirect, allowed (forbidden) transitions $\nu = 2$ ($\nu = 3$). We have used $\nu = 2$ for the present nano-crystalline or amorphous films according to Ref. [33]. Near the absorption edge, T_0 and C are approximately constant and the E_g value of all the TiO₂ samples is obtained (see Table 1) by fitting the absorption edge with Eq. (1) (inset of Fig. 4). The value of band gap of 3.12 eV lies in between the theoretical values of anatase (3.2 eV) and rutile (3.0 eV) phase, thus signaling the presence of mixed anatase–rutile phase in undoped TiO₂. For N-doped TiO₂ a slight change in band gap (3.0 eV) is observed. In the case of V-doped TiO₂, the tail of absorption edge is clearly shifted to 2.8 eV while significant narrowing to 2.5 eV of band gap is observed for V–N codoped TiO₂. This result indicates that higher visible light absorption can be achieved by codoping.

Theoretical studies were carried out using DFT with GGA + mBJ potentials to understand the noticeable decrease in the band gap of TiO₂ after co-doping. The concentration used in the present experiments (1 at% V and 2 at% N) were chosen for the theoretical studies. Fig. 5 represents the calculated total density of states (DOS) of pure, mono-doped, and codoped TiO₂. For pure TiO₂, Fermi energy (E_F) is set to 0 eV while for the other systems highest occupied electronic states of TiO₂ is considered as a reference point and shifted to 0.0 eV, while E_F is represented by dotted line. It is seen that for n-type (V) doping in TiO₂, E_F is shifted close to CBM while for p-type (N) doping, E_F is close to VBM. While, V+2N doping (due to net p-type doping) again shifts the E_F close to VBM. Additional DOS due to dopants are clearly observed for mono-doped and codoped TiO₂ within the band gap region. In order to understand the origin of these electronic levels, partial density of states (PDOS) for all the four TiO₂ systems (pure, N-doped, V-doped, and V–N codoped TiO₂) is plotted in Fig. 6. Here, position of E_F is also shifted as in the case of Fig. 5. Pure TiO₂ (Fig. 6a) shows the band gap of 2.9 eV which is within 10% variation with the experimental band gap (3.2 eV) (DFT

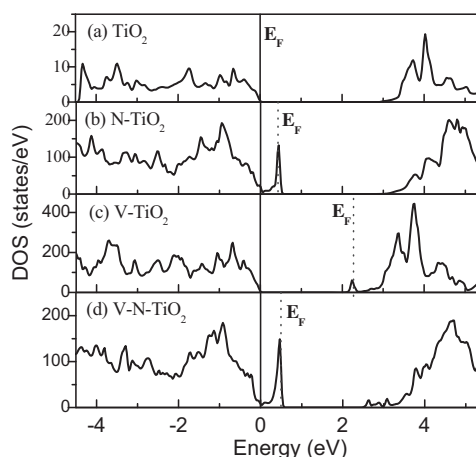


Fig. 5. Total density of states of (a) pure anatase TiO₂, (b) N–TiO₂, (c) V–TiO₂ and (d) V–N–TiO₂.

with mBJ potential produces results within 10% of experimental values). From PDOS, the valence bands (VB) are mainly dominated by O 2p states while conduction bands are contributed by Ti-3d states ($e_g + t_{2g}$) with major contribution by t_{2g} electrons. In the case of N-doped TiO₂ (Fig. 6b), N 2p states are localized just above the valence band maxima (VBM) which overlaps with VB to shift the VBM to higher energy by 0.1 eV with respect to pure TiO₂ (Fig. 6b). This narrowing is in good agreement with that obtained experimentally. Some fraction of N 2p states are hybridized with the O 2p states in the valence region while the CB is still dominated by Ti 3d (mainly e_g) states. For V-doped TiO₂ (Fig. 6c), isolated energy states of e_g electron of V 3d orbitals are formed at 0.7 eV below the conduction band minima (CBM) of pure TiO₂ (Fig. 6a). While the valence bands are still dominated by O 2p states, hybridization of V and Ti 3d states is also observed in lower conduction band region. For V doping the contribution of Ti 3d (t_{2g}) orbitals increases which may be due to the change in Ti valance states ($Ti^{4+} \rightarrow Ti^{3+}$). In the case of V–N codoped TiO₂, the VB mostly consists of O 2p and N 2p states, while CB is dominated by Ti 3d (e_g) and V 3d (t_{2g}) states (Fig. 6d). On the other hand, the impurity energy levels due to N 2p and V 3d (e_g) states are formed just above the VBM and below the CBM, respectively. As compared to single-element doped TiO₂ a slight variation in the position in the isolated energy levels created by V and N in TiO₂ band gap is observed due to the interaction of V 3d and N 2p orbitals. It is also observed that the lowering of CBM is reduced in comparison to V-doped TiO₂ which can be ascribed to the occupancy of N-ions in oxygen vacancy sites generated by V-doping. This shows that maximum narrowing of the band gap obtained with V–N codoped TiO₂ is mainly attributed to the formation of impurity energy states near both the band edges. While for monodoped TiO₂ the narrowing of the band gap is only contributed by impurity level formed near any one of the band edges.

The photocatalytic activity of pure, N-doped, V-doped, and V–N codoped TiO₂ thin films was tested by examining the degradation of organic pollutants as a function of time. The decrease of relative concentration of the 4-CP, 4-NP, MB dye was estimated by measuring the relative intensity of the peak at 225, 320, and 664 nm from the optical absorbance spectra, respectively. Langmuir–Hinshelwood model usually describes the photo-degradation reaction of organic pollutants. The apparent reaction rate constant (k) of the model was obtained from the slope of the $\ln(C/C_0)$ vs irradiation time plot (Fig. 7). All the data points of Fig. 7 were well fitted linearly indicating that all photo-degradation reactions follow first order kinetics. Thus the diffusion of organic molecules on the catalyst surface is the rate limiting step during the degradation reaction. All the TiO₂ photo-catalyst samples were

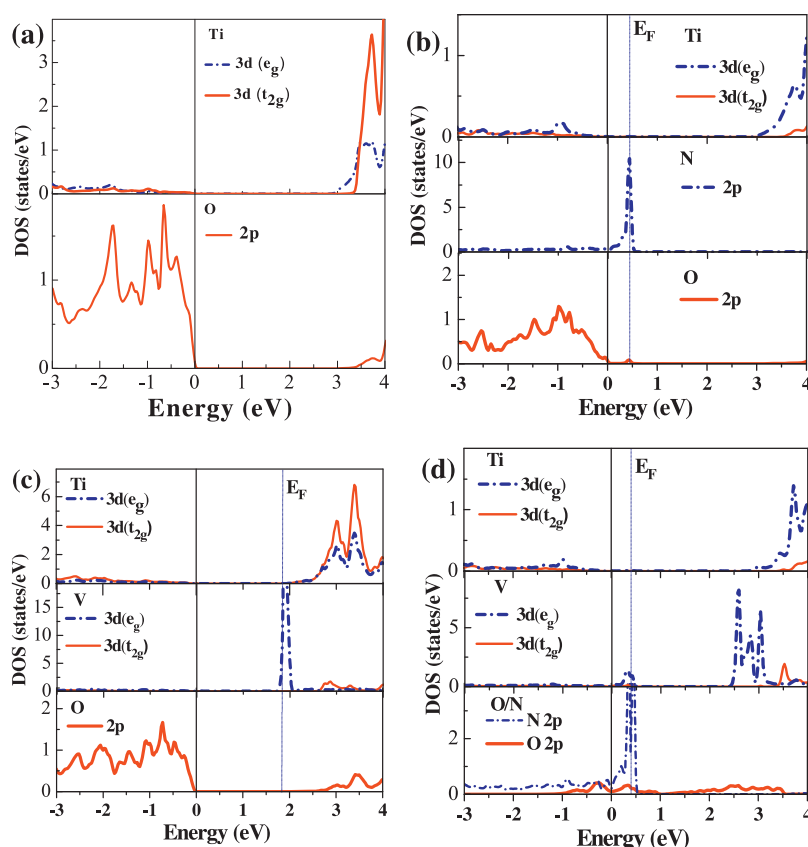


Fig. 6. Partial density of states for (a) pure anatase TiO_2 , (b) N-TiO_2 , (c) V-TiO_2 , (d) V-N-TiO_2 .

able to completely (100%) degrade each organic pollutants with doped TiO_2 showing better photocatalytic activity than undoped TiO_2 , irrespective of the type of dopant used. Most importantly, V–N codoped TiO_2 films were able to degrade all the three organic pollutants much faster than mono-doped and undoped TiO_2 in the presence of visible light. The value of k (Table 1) increases moving from pure TiO_2 to N-doped, to V-doped, to V–N codoped TiO_2 . The codoped TiO_2 is able to degrade 4-CP, 4-NP, and MB dye with 1.9, 2.8, and 2.6 times higher rate than undoped TiO_2 , respectively.

During the photocatalytic reaction, TiO_2 absorbs light to produce electron–hole pair which migrates to the catalyst surface to react with absorbed O_2 and H_2O , to produce strong oxidizing agents in the form of $\text{O}_2^{\cdot-}$ and OH^{\cdot} radicals, respectively, which are the main species responsible for the degradation of organic pollutants [1]. Thus the production of good number of electron–hole pairs, fast transfer of these pairs to the catalyst surface before recombination and sufficient absorption of organic pollutants on the catalyst surface are the rate limiting factors for degradation. In case of V–N codoped TiO_2 , impurity energy levels are created below the CBM and above the VBM by V and N dopants, respectively, in the band gap of TiO_2 to cause the absorption edge to shift into visible region as compared to mono-doped TiO_2 . Thus by increasing the ability to absorb photons, large numbers of photo-generated charges are generated to enhance the degradation rate of pollutants. When doped with the optimum concentration, these impurity energy levels also act as the trapping sites for the photo-generated charges. N species, because of the charge imbalance between oxygen and nitrogen ions, act as hole trapping sites to decrease the recombination process [5]. Similarly for V-dopant, V^{4+} ions are present in the substitutional site of Ti^{4+} in TiO_2 lattice, while V^{5+} ions are present on the surface of TiO_2 in the form of V_2O_5 species which

have lower Fermi level that favors the fast transfer of electrons from CB of TiO_2 to V^{5+} ions leaving back holes [19,28]. This results in the effective separation of electron and holes. However, optimum concentration of these dopants must be incorporated into TiO_2 because above the optimum concentration the same trapping sites act in the opposite way, i.e. as charge recombination centers. In the case of V–N-codoped TiO_2 , optimum V (1 at%) and N (2 at%) (data from XPS) content helps to efficiently separate the photo-generated charges by acting as trapping sites for the electrons and holes, respectively. Thus, the probability of photo-generated charges to reach the catalyst surface before recombination is far better for codoped- TiO_2 than mono-doped TiO_2 . Mixed phase of anatase-rutile present in the TiO_2 films produces synergetic effect to enhance the photocatalytic activity [34]. The antenna effect created by rutile is able to improve the photo-reactivity by decreasing the recombination rate of the generated charges [35,36]. However, optimum content of anatase and rutile phase should be present in the mixture to achieve high photocatalytic activity. Lei and Duan [34] and Coa et al. [37] showed that TiO_2 with mixed phase containing 60% to 40% of anatase provide the highest degradation rate for the pollutants. Accordingly to Table 1, the weight fraction of anatase phase (41%) for V–N codoped TiO_2 lies just in this optimum range to create ideal condition for the photo-degradation of the organic pollutants. These are the main reasons responsible for higher photocatalytic activity for the degradation of organic pollutants in V–N codoped TiO_2 film.

Most important advantage of photo-catalyst in form of thin film is that it can be recovered and reused with minimum effort and thus can be used as ON/OFF switch for the catalytic reaction. To study this particular property, the V–N codoped TiO_2 thin film photo-catalyst was recycled 4 times for the degradation of MB dye in the presence of visible light (Fig. 8). The degradation rate was decreased by small

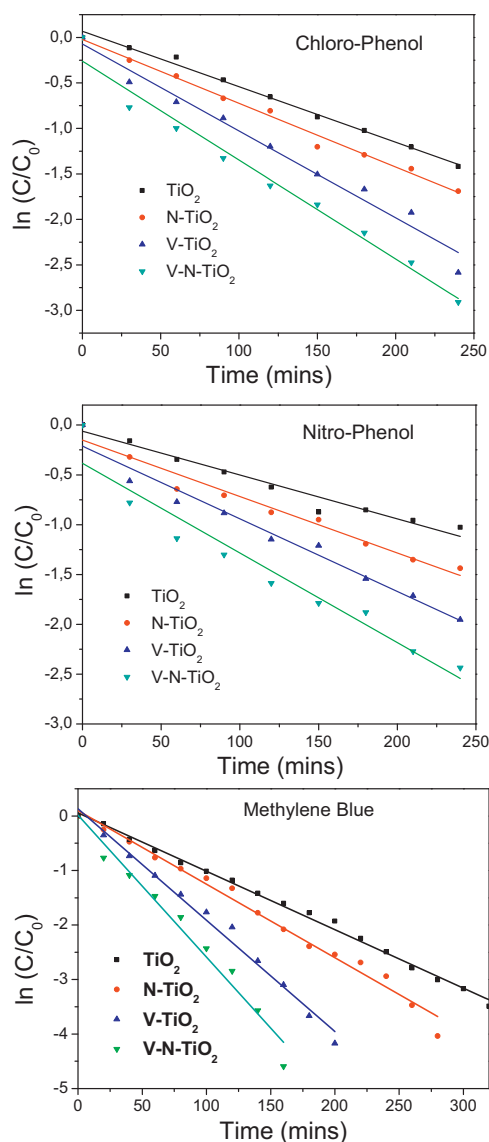


Fig. 7. Time dependent photocatalytic degradation ratio of 4-CP, 4-NP, and MB solution in presence of visible light using pure TiO_2 , N-doped TiO_2 , V-doped TiO_2 and V–N codoped TiO_2 thin films.

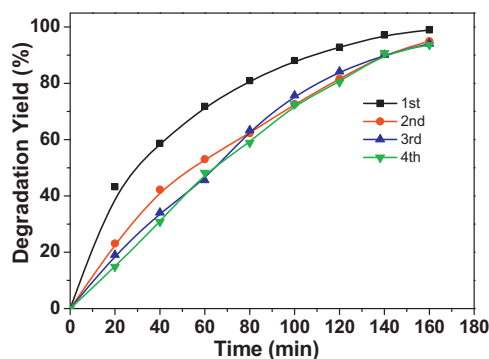


Fig. 8. Cyclic behavior of V–N codoped TiO_2 thin films for degradation of MB dye in presence of visible light.

amount in the 2nd run but no further decrease in photocatalytic performance was observed in 3rd and 4th run.

4. Conclusion

Pure, N-doped, V-doped and V–N codoped TiO_2 thin films have been deposited by using RF-magnetron sputtering to decrease both the band gap and the recombination rate of the electron–hole pairs in pure TiO_2 . V–N codoped TiO_2 films showed maximum narrowing of the band gap in the visible region (2.5 eV) as compared to single-element doped (2.8 for V-doped and 3.0 eV for N-doped) or undoped TiO_2 (3.12 eV). This shows that maximum narrowing of the band gap obtained with V–N codoped TiO_2 is mainly attributed to the formation of impurity energy states near both the band edges of V 3d and N 2p orbitals.

Density of states calculated by DFT contributed to better understand the band gap narrowing in codoped TiO_2 that is indeed attributed to the formation of isolated energy level of V 3d and N 2p states below the conduction band and above the valence band, respectively. While for mono-doped TiO_2 the narrowing of the band gap is only contributed by impurity levels formed near any one of the band edges. Chemical states of dopants studied with XPS proved that for N-doped TiO_2 , N occupies only interstitial sites in the lattice, while codoping with V permits N to reside in both substitutional and interstitial sites in TiO_2 lattice which induces higher visible light sensitivity.

The new energy levels created by doping and codoping are also responsible for better charge separation by acting as trapping sites. The codoped TiO_2 is able to degrade 4-CP, 4-NP and MB with 1.9, 2.8 and 2.6 times higher rate than undoped TiO_2 , respectively. In conclusion, the photocatalytic activity of V–N-codoped TiO_2 thin film, higher than that of undoped or mono-doped films, is attributed to both lower energy band gap and reduced charge recombination rate.

Acknowledgement

We acknowledge C. Armellini for the support in the XRD analysis, E. Moser for support in the Raman measurements, C. Cestari for arrangement of lamp set up. The research activity is partially supported by 7th UE research programme (Marie Curie Action, PAT-COFUND) as well as by the PAT-project ENAM in cooperation with Istituto MCB of CNR (Italy). The research activity is also partially supported by UGC-UPE (India) Green Technology Project. One of us (A.D.) is thankful to SERB (DST), New Delhi, India for research grant (SR/FTP/PS-063/2011).

References

- [1] W.G. Kuo, *Water Res.* 26 (1992) 881–886.
- [2] F.B. Li, X.Z. Li, *Appl. Catal., A* 228 (2002) 15–27.
- [3] A. Fujishima, X. Zhang, D.A. Tryk, *Surf. Sci. Rep.* 63 (2008) 515–582.
- [4] M. Ni, M.K.H. Leung, D.Y.C. Leung, K. Sumathy, *Renewable Sustainable Energy Rev.* 11 (2007) 401–425.
- [5] Y. Cong, J.L. Zhang, F. Chen, M. Anpo, *J. Phys. Chem. C* 111 (2007) 6976–6982.
- [6] J. Zhu, Z. Deng, F. Chen, J. Zhang, H. Chen, M. Anpo, *Appl. Catal., B* 62 (2006) 329–335.
- [7] R. Dholam, N. Patel, A. Miotello, *Int. J. Hydrogen Energy* 36 (2011) 6519–6528.
- [8] X.H. Wang, J.G. Li, H. Kamiyama, Y. Moriyoshi, T. Ishigaki, *J. Phys. Chem. B* 110 (2006) 6804–6809.
- [9] R. Asahi, T. Morikawa, T. Ohwaki, K. Aoki, Y. Taga, *Science* 293 (2001) 269–271.
- [10] S.U.M. Khan, M. Al-shahry, W.B. Ingler, *Science* 297 (2002) 2243–2245.
- [11] T. Umebayashi, T. Yamaki, H. Itoh, K. Asai, *Appl. Phys. Lett.* 81 (2002) 454–456.
- [12] R. Dholam, N. Patel, M. Adami, A. Miotello, *Int. J. Hydrogen Energy* 34 (2009) 5337–5346.
- [13] D. Li, N. Ohashi, S. Hishita, T. Kolodiazhnyi, H. Haneda, *J. Solid State Chem.* 178 (2005) 3293–3302.
- [14] J. Liu, R. Han, Y. Zhao, H. Wang, W. Lu, T. Yu, Y. Zhang, *J. Phys. Chem. C* 115 (2011) 4507–4515.
- [15] D.E. Gu, B.C. Yang, Y.D. Hu, *Catal. Commun.* 9 (2008) 1472–1476.

- [16] C. Wen, Y.J. Zhu, T. Kanbara, H.Z. Zhu, C.F. Xiao, *Desalination* 249 (2009) 621–625.
- [17] Y. Xie, Q.N. Zhao, X.J. Zhao, Y.Z. Li, *Catal. Lett.* 118 (2007) 231–237.
- [18] D. Chen, Z. Jiang, J. Geng, Q. Wang, D. Yang, *Ind. Eng. Chem. Res.* 46 (2007) 2741–2748.
- [19] R. Jaiswal, N. Patel, D.C. Kothari, A. Miotello, *Appl. Catal., B* 126 (2012) 47–54.
- [20] P. Blaha, K. Schwarz, G.K.H. Madsen, D. Kvasnicka, J. Luitz, Wien2K Code, An Augmented Plane Wave Plus Local Orbitals Program for Calculating Crystal Properties, Vienna University of Technology, Vienna, Austria, 2012.
- [21] J.P. Perdew, A. Ruzsinszky, G.I. Csonka, O.A. Vydrov, G.E. Scuseria, L.A. Constantin, X. Zhou, K. Burke, *Phys. Rev. Lett.* 100 (2008) 136406, *ibid.* 2009 102 039902 (E).
- [22] F. Tran, P. Blaha, *Phys. Rev. Lett.* 102 (2009) 226401–226404.
- [23] A. Rubio-Ponce, A. Conde-Gallardo, D. Olguín, *Phys. Rev. B: Condens. Matter* 78 (2008) 035107–35109.
- [24] F.C. Gennari, D.M. Pasquevich, *J. Am. Ceram. Soc.* 82 (1999) 1915–1921.
- [25] K. Yanagisawa, J. Ovenstone, *J. Phys. Chem. B* 103 (1999) 7781–7787.
- [26] X.F. Chen, X.C. Wang, Y.D. Hou, J.H. Huang, L. Wu, X.Z. Fu, *J. Catal.* 255 (2008) 59–67.
- [27] T. Horikawa, M. Katoh, T. Tomida, *Microporous Mesoporous Mater.* 110 (2008) 397–404.
- [28] H. Liu, G. Liu, X. Shi, *Colloids Surf., A* 363 (2010) 35–40.
- [29] X. Ma, L. Miao, S. Bie, J. Jang, *Solid State Commun.* 150 (2010) 689–692.
- [30] B.M. Reddy, P.M. Sreekanth, E.P. Reddy, *J. Phys. Chem. B* 106 (2002) 5695–5700.
- [31] X. Yang, F.Y. Ma, K.X. Li, Y.N. Guo, J.L. Hu, M.X.W. Huo, H.J. Guo, *J. Hazard. Mater.* 175 (2010) 429–438.
- [32] W. Lohstroh, R.J. Westerwaal, V.J.L.M. Mechelen, C. Chacon, E. Johansson, B. Dam, R. Griessen, *Phys. Rev. B: Condens. Matter* 70 (2004) 165411–165511.
- [33] E.A. Davis, N.F. Mott, *Philos. Mag.* 22 (1970) 903–922.
- [34] S. Lei, W. Duan, *J. Environ. Sci.* 20 (2008) 1263–1267.
- [35] T. Kawahara, Y. Konishi, H. Tada, N. Tohge, J. Nishii, S. Ito, *Angew. Chem. Int. Ed* (2002) 2811–2813.
- [36] D.C. Hurum, A.G. Agrios, K.A. Gray, T. Rajh, M.C. Thurnauer, *J. Phys. Chem. B* 107 (2003) 4545–4549.
- [37] W. Zhang, T. Zhang, W. Yin, G. Cao, *J. Chin. Chem. Phys.* 20 (2007) 95–98.